

Chiral Quasi-Bound States in the Continuum

Adam Overvig^{1,2}, Nanfang Yu,^{2,†} and Andrea Alù^{1,3,*}

¹*Photonics Initiative, Advanced Science Research Center at the Graduate Center of the City University of New York, New York, New York 10031, USA*

²*Department of Applied Physics and Applied Mathematics, Columbia University, New York, New York 10027, USA*

³*Physics Program, Graduate Center, City University of New York, New York, New York 10016, USA*



(Received 8 June 2020; accepted 13 January 2021; published 17 February 2021)

Quasi-bound states in the continuum (QBICs) are Fano resonant states with long optical lifetimes controlled by symmetry-breaking perturbations. While conventional Fano responses are limited to linear polarizations and do not support tailored phase control, here we introduce QBICs born of chiral perturbations that encode arbitrary elliptical polarization states and enable geometric phase engineering. We thereby design metasurfaces with ultrasharp spectral features that shape the impinging wave front with near-unity efficiency. Our findings extend Fano resonances beyond their conventional limits, opening opportunities for nanophotonics, classical and quantum optics, and acoustics.

DOI: [10.1103/PhysRevLett.126.073001](https://doi.org/10.1103/PhysRevLett.126.073001)

Suitably designed photonic crystal slabs (PCSs) have been recently shown to support quasi-bound states in the continuum (QBICs): Fano resonant modes whose radiative lifetime is controlled by symmetry-lowering perturbations [1] that become nonradiating states [2–4] due to symmetry protection in the absence of the perturbation. When light with a polarization state matching the QBIC eigenpolarization impinges on the structure, an ultrasharp Fano response arises [5], and the resonantly scattered light maintains the same polarization. This property, combined with strong in-plane Bragg scattering in high-contrast index systems [6], enables compact optical devices concentrating light in both space and time [7–11]. By perturbing every other unit cell in such systems, the Brillouin zone folds, enabling access to previously bound modes and providing additional design freedom to control QBICs in real and momentum space [10–13]. Photonic crystals supporting QBICs, hence, offer a highly versatile platform for biological sensing [14], planar optical modulators [15], notch filters [16], and nonlinear optics [17,18].

Recently, the selection rules for QBICs in planar photonic crystals have been classified, clarifying to which (if any) free-space polarization state a QBIC couples due to a chosen symmetry perturbation [13]. This result implies that the QBIC polarization must be linear in planar structures that preserve symmetry across a horizontal plane. Adiabatically varying this polarization angle in the lateral direction introduces a spatially varying geometric phase, enabling metasurface functionalities such as anomalous reflection and refraction for circularly polarized light [13]. However, due to the planarized symmetry and the linear polarization constraint, the maximum achievable efficiency of wave front shaping is 25% [19].

Breaking this symmetry with the introduction of optical chirality may enable devices with strong circular dichroism [20–29]. A common approach to achieve strong optical chirality is the spectral superposition of two modes supported by structures with intrinsic geometrical asymmetries [30,31]. Recent work has demonstrated metasurfaces that vary the geometric phase associated with spin-preserving chiral structures in devices with asymmetric transmission profiles [32–34]. In parallel, the emerging field of twistronics has been exploring how anisotropic parallel layers stacked with a twist with respect to one another can exhibit unexpected electronic [35] and optical [36,37] properties pertaining to the eigenstates of the composite system, opening new degrees of freedom in engineering wave-matter interactions.

Motivated by these recent advances, in this Letter, we show that a pair of tightly stacked interfaces, each with a distinct perturbation, can support Fano resonances born of chiral QBICs: spectrally isolated, nondegenerate modes whose coupling to free space is intrinsically chiral. As in other QBIC systems, the perturbation weakly alters the mode so that it leaks to free space with a scattering rate determined by the magnitude of the perturbation and to a polarization state determined by symmetry (i.e., governed by selection rules). Unlike conventional QBICs, however, which are limited to linear polarizations and a fixed phase response, we show that this polarization state can be arbitrarily elliptical with any desired phase at resonance. The resulting Fano resonances exhibit designer elliptical dichroism, engineerable with complete and continuous coverage of the Poincaré sphere. In particular, circularly polarized light may be selected with any in-plane orientation, resulting in a spin-selective Fano resonance encoding

arbitrary geometric phase. Our finding enables Fano resonant metasurfaces that can shape an impinging wave front with near-unity efficiency (spin selectivity) exclusively across a designer bandwidth of choice (spectral selectivity). Since these concepts originate solely from symmetry perturbations, we anticipate their extension to other physical domains supporting Fano resonances, such as at radio frequencies or in acoustics.

Consider a slab supporting a symmetry-protected BIC controlled by two homogenized interfaces, engineered to scatter the trapped energy to the far field by breaking a relevant symmetry. We assume that the bottom and top interfaces scatter light to linear polarization states oriented at angles ϕ_1 and ϕ_2 , respectively, where in the achiral case $\phi_1 = \phi_2$ due to symmetry, while in the general chiral case [Fig. 1(a)] ϕ_1 and ϕ_2 are different. Based on temporal coupled mode theory (TCMT) [38,39], we can write the states leaking upward and downward, respectively, as

$$\begin{aligned} |e_u\rangle &= \frac{1}{\sqrt{\tau}} \left\{ \mp \begin{bmatrix} \cos(\phi_1) \\ \sin(\phi_1) \end{bmatrix} + i \begin{bmatrix} \cos(\phi_2) \\ \sin(\phi_2) \end{bmatrix} \right\}, \\ |e_d\rangle &= \frac{1}{\sqrt{\tau}} \left\{ i \begin{bmatrix} \cos(\phi_1) \\ \sin(\phi_1) \end{bmatrix} \mp \begin{bmatrix} \cos(\phi_2) \\ \sin(\phi_2) \end{bmatrix} \right\}, \end{aligned} \quad (1)$$

where τ is the optical lifetime of the mode controlled through the magnitude of the symmetry perturbation, the top (bottom) sign corresponds to the symmetric (anti-symmetric) mode in the z direction, and the factor i accounts for the relative scattering phase of the top and bottom interfaces [38].

Such metasurfaces may be implemented with properly chosen perturbations applied to otherwise high-symmetry PCSs: In Fig. 1(b), an unperturbed periodic permittivity profile H^0 (circular holes etched in a high-index slab) is successively perturbed into structures V_1 at the bottom interface (two ellipses oriented at α and $\alpha + 90^\circ$) and V_2 at the top interface (two ellipses oriented at $\alpha + \Delta\alpha$ and $\alpha + \Delta\alpha + 90^\circ$). The period in one direction is doubled from a to $2a$ due to this perturbation, allowing excitation of modes that were previously guided [11]. When $\Delta\alpha$ is properly chosen so that $\phi_2 = \phi_1 \pm \pi/2$, the leaking states are right-handed circularly polarized (RCP). Hence, upon excitation by a plane wave at normal incidence (from either below or above), the device shows full circular dichroism: RCP light is resonantly reflected, and left-handed circularly polarized (LCP) light is nonresonantly transmitted [Fig. 1(c)].

Both spectral selectivity (linewidth) and spin selectivity (handedness) of the optical response originate from and are controllable through the symmetry perturbation. To demonstrate this, Figs. 1(d) and 1(e) show three-dimensional schematics of the unperturbed and perturbed geometry [whose spectra are shown in Fig. 1(c), calculated by finite difference time domain simulations (Lumerical Solutions)]. Here, a thin Si film of height $h = 1.25a$ and refractive index $n = 3.45$ is suspended in SiO_2 , with refractive index $n_0 = 1.45$, filling circular inclusions with diameter D_0 [Fig. 1(d)] or elliptical inclusions [Fig. 1(e)] with diameters $D_0 \pm \delta/2$ (δ quantifies the magnitude of the perturbation). We note that such a structure may be manufactured by multistep lithography and planarization at telecommunications wavelengths [40,41]. The quasi-TE mode supported by the unperturbed structure is bound to the slab [Fig. 1(f)], and it is characterized by a vertically antisymmetric out-of-plane magnetic field H_z [corresponding to the bottom sign in Eq. (1)]. Upon perturbation [Fig. 1(g)], the H_z profile is weakly perturbed such that an induced chiral moment scatters light upward and downward as RCP waves (demonstrated by the quantities $H_x \pm iH_y$, where the complex conjugation reflects a change in direction, not handedness). The device in Fig. 1(e) thereby supports a chiral QBIC: a long-lived optical state that, by construction, has a Q factor varying as $Q \propto 1/\delta^2$ [1] and selection rules

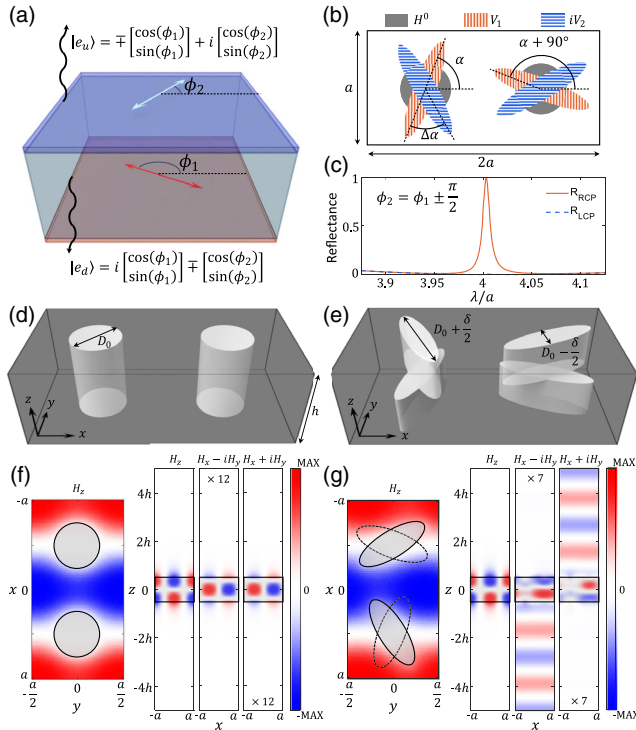


FIG. 1. Chiral QBICs. (a) Homogenized model of a metasurface supporting a chiral QBIC: Two interfaces scatter optical energy to linearly polarized free-space light with polarization angles ϕ_1 and ϕ_2 , respectively, resulting in chiral states leaked upward and downward, $|e_u\rangle$ and $|e_d\rangle$. (b) Perturbation scheme involving two perturbations, V_1 and V_2 , for control over ϕ_1 and ϕ_2 , respectively. (c) Example spectra of a device based on the scheme in (b) (with $\alpha = 70^\circ$ and $\Delta\alpha = 50^\circ$) showing full circular dichroism only at resonance. (d),(e) Unperturbed and perturbed structures, respectively. (f),(g) Unperturbed and perturbed magnetic field components, showing that the bound state (principally characterized by H_z) leaks to RCP light when perturbed.

that are intrinsically chiral, leaking exclusively to a single circular polarization channel.

In particular, the selection rules of each interface prescribe coupling to light polarized at angles ϕ_1 (following $\phi_1 \approx 2\alpha$) for V_1 and ϕ_2 (following $\phi_2 \approx 2(\alpha + \Delta\alpha)$) for V_2 [13,38]. Upon insertion into Eq. (1), this implies that the orientation angles of the real and imaginary parts of the scattered light are separately and arbitrarily controlled, and, hence, elliptical dichroism is possible. This is shown in Fig. 2 by varying $\Delta\alpha$ from -90° to 90° and α from 0° to 90° and studying the eigenpolarizations of the corresponding QBICs by analyzing the Jones matrix for the transmitted light at the resonant frequency. As an example, Fig. 2(a) maps the peak reflectance R for the metasurface in Fig. 1(e) with $\alpha = 47^\circ$ and $\Delta\alpha = 31^\circ$ as a function of the ellipticity parameters of the polarization state 2χ and 2ψ , representing the latitude and longitude on the Poincaré sphere, respectively. We find a peak with near-unity reflectance (marked with a red dot) and with near-unity transmittance (marked with a blue dot) at the resonant frequency. Figure 2(b) shows the reflectance spectra for these two extremal cases, demonstrating a Fano resonance for one of the eigenpolarizations and minimal response for the orthogonal state. The inset shows that the eigenpolarization maintains its polarization state, including its handedness, upon reflection. The values of 2χ and 2ψ may be determined

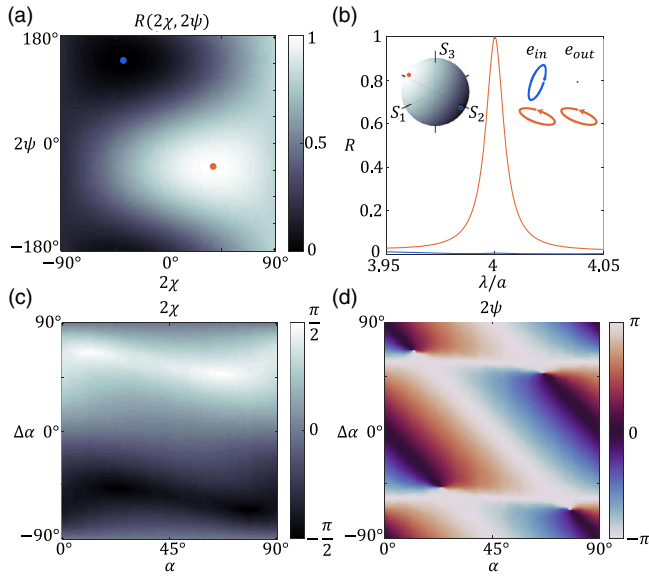


FIG. 2. Fano resonances with arbitrary elliptical eigenpolarizations. (a) Map of reflectance for a device with $\alpha = 47^\circ$ and $\Delta\alpha = 31^\circ$ as a function of the input polarization state (characterized by the latitude 2χ and longitude 2ψ on the Poincaré sphere). (b) Reflectance spectra for the extremal cases in (a) (marked by red and blue dots), with the insets showing the eigenpolarization states e that are maximally and minimally resonant and their positions on the Poincaré sphere. (c),(d) Map of the coverage of the Poincaré sphere for the maximally resonant elliptical eigenpolarization as a function of α and $\Delta\alpha$.

for every choice of $\Delta\alpha$ and α using a similar procedure and are shown in Figs. 2(c) and 2(d). Hence, by varying the metasurface geometry, we can span the Poincaré sphere, with 2χ controlled by $\Delta\alpha$ and 2ψ controlled by both α and $\Delta\alpha$ [38].

Next, we study metasurfaces designed for RCP illumination where the elliptical eigenpolarization is spatially varied across the device. We begin by building a library of metaunits (the building blocks of a spatially varying metasurface) capable of controlling both the amplitude and phase of the resonantly reflected RCP light, comparable to the results in Ref. [42] but applied only across the designed bandwidth of the QBIC. For RCP light incident on a device with eigenpolarization $|e\rangle$, the complex amplitude of the RCP component of the reflected wave is

$$E_R = \langle e|R \rangle^2 = \frac{1}{2} [1 + \sin(2\chi)] e^{2i\psi}. \quad (2)$$

The remaining states (LCP in reflection and LCP and RCP in transmission) may be easily written as well [38]. The amplitude of reflected RCP light, therefore, varies from 0 to 1 as 2χ varies from $-\pi/2$ to $\pi/2$ (the poles of the Poincaré sphere), while the phase is $\Phi = 2\psi$. According to the relation between 2ψ and α in Fig. 2(d), the phase of the reflected RCP light varies as $\Phi \sim 4\alpha$.

Full-wave simulations (Lumerical Solutions) confirm this picture: Fig. 3(a) shows how the spectral reflectance for RCP light can arbitrarily vary between zero and unity by simply changing $\Delta\alpha$, and Fig. 3(b) shows that the spectral phase function can be substantially controlled to allow any

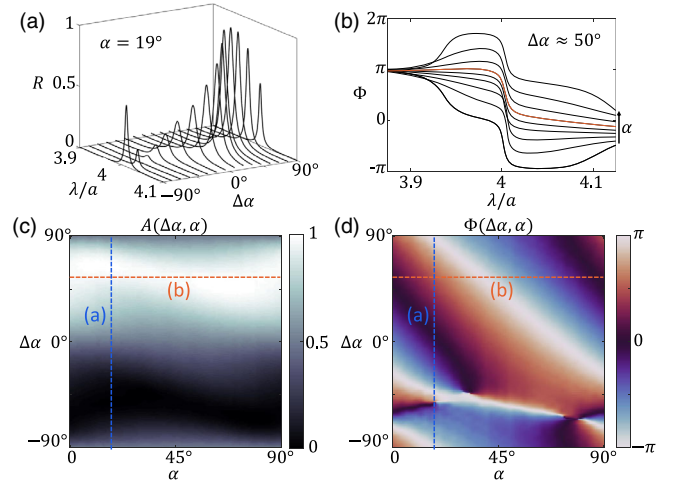


FIG. 3. Full control over the amplitude and phase of resonantly reflected light. (a) Spectral reflectance near the resonance for $\alpha = 19^\circ$ and sampled values of $\Delta\alpha$. (b) Spectral phase near the resonance for $\Delta\alpha \approx 50^\circ$ and sampled values of α . The orange curve highlights the conventional phase function expected for a Fano resonance. (c),(d) Amplitude A and phase Φ at the resonant wavelength for reflected RCP light as a function of α and $\Delta\alpha$, with the contours sampled in (a),(b) highlighted.

phase value at resonance by varying α , markedly different from a conventional resonant metasurface. Figures 3(c) and 3(d) map the amplitude and phase of reflected RCP light as a function of α and $\Delta\alpha$, showing that we can achieve any desired value. In Supplemental Material [38], we invert this information to create a look-up table prescribing the geometry that achieves any desired complex reflection coefficient. This tool is ideal to apply the concept of geometric phase to a chiral QBIC metasurface with slow variations of amplitude and phase in its transverse plane synthesizing arbitrary wave fronts with large efficiency. Compared to conventional Fano resonances and metasurfaces, chiral QBICs enable highly efficient transformations exclusively across controllable linewidths while remaining fully transparent for other frequencies.

Figure 4 demonstrates, as an example, a phase-gradient chiral QBIC metasurface anomalously reflecting incoming RCP light with near-unity efficiency only at resonance (with near-zero efficiency off resonance). We construct a sublibrary of Fig. 3 with maximal amplitude and complete phase coverage, seen in Fig. 4(a)[38]. This sublibrary provides a spatial phase gradient by varying α ; linearly varying the phase across a superperiod of $16a$ results in a metasurface that generates a tilted plane wave with in-plane momentum $k_g = \pm\pi/8a$ [Fig. 4(b)]. Because of this additional momentum imparted during the scattering process,

when excited from normal incidence a spatially varying dark mode is observed with a Bloch wave vector k_g [shown overlaid with the geometry in Fig. 4(c)]. This encoded momentum is imparted upon coupling both in and out [19], meaning that the outgoing light is deflected by a total of $2k_g$. The far field for each wavelength is shown in Fig. 4(d) and 4(e) for RCP and LCP light, respectively, demonstrating near-unity anomalous reflection when RCP light is incident and near-unity specular transmission when LCP light is incident.

Notably, despite the presence of nine distinct diffraction orders for each polarization state in both transmission and reflection sides, the metasurface supports a sharp Fano resonance with near-unity reflectance to an arbitrary angle (the $m = \pm 2$ diffraction order). This behavior stands in stark contrast to conventional Fano metasurfaces, wherein additional diffraction orders act as significant loss pathways in the scattering process. The period of the structure is typically made sufficiently subwavelength to support only two diffraction orders [11], avoiding unwanted energy pathways and guaranteeing unity reflectance in the absence of material loss. This discrete translational symmetry is necessarily broken in our system in order to impart the phase gradient, and yet, since our system is constructed by weakly perturbing a zeroth-order grating, it maintains the very large efficiency while offering a designer phase profile that selects which angles are involved in the Fano resonance. Conservation of linear momentum would preclude all but four orders ($m = 0$ and $m = \pm 2$, with the sign determined by the spin) [19], but the resulting achirality results in a system with a maximum of 25% diffraction efficiency that necessarily splits the resonant light into four channels according to the spin [38]. Here, in contrast, spin selectivity eliminates the pathways corresponding to the nonresonant circular polarization, realizing a true two-port generalized Fano resonance with wave-front-shaping functionality and coupling to a single output channel with near-unity efficiency.

More complex wave front shaping, such as focusing or orbital angular momentum generation, is generally possible following similar principles. The library in Fig. 3 enables arbitrary phase-amplitude holography encoded in a chiral QBIC and optically reconstructable only using the correct input polarization and wavelength; all nonresonant wavelengths will see a slab acting as a weakly perturbed effective medium. In total, a chiral QBIC enables engineering with large flexibility the Fano resonance Q factor, resonant wavelength, and phase-amplitude response simultaneously by tuning the magnitude of the perturbation, unperturbed lattice geometry, and orientation angles of the chiral structure, respectively. Notably, unlike recent demonstrations of polarization vortices born of BICs [43,44], the control of the QBIC properties is here in real space rather than in momentum space. As a consequence, spatial variations of the phase-amplitude response directly

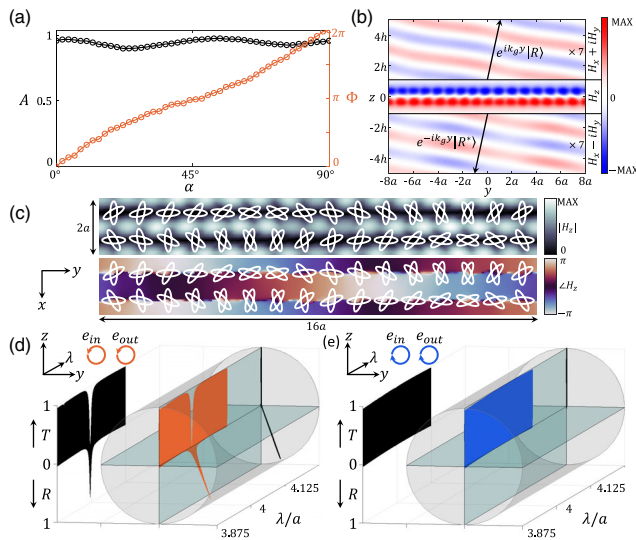


FIG. 4. Chiral phase-gradient resonant metasurface with near-unity diffraction efficiency. (a) Sublibrary of Figs. 3(c) and 3(d) with near-unity amplitude and phase varying over 2π . (b) Device with a spatially tailored leaky mode encoding a coupling phase gradient of $k_g = \pi/8a$. (c) Mode profile on resonance when excited at normal incidence. The ellipses denote the geometry of the structure. (d) Far field for RCP incidence at each wavelength, demonstrating near-unity diffraction efficiency (96.1%) to the anomalously reflected angle (20.17°). The spin is preserved in transmission and reflection. (e) Far field for LCP incidence at each wavelength, showing no resonance.

translate into control of the local diffraction angles and diffraction efficiencies and are thereby applicable to finite-sized beams with a large spread of momentum [19]. The approach outlined here therefore drastically advances the control of Fano resonances with spatially tailored dark modes, establishing an exciting platform for applications such as augmented reality and secure optical communications, which enable a broadband transparent response unless interrogated in a very narrow spectral range with a specific eigenpolarization of choice.

In conclusion, we have shown that Fano responses are not bound to linear polarizations and specific amplitude and phase response at resonance. By introducing QBICs based on chiral symmetry perturbations, we have expanded the range of available eigenpolarization states for ultrasharp resonances to the entire Poincaré sphere. When the eigenpolarization is circularly polarized, the device supports a Fano resonance exhibiting full circular dichroism, for which the resonant eigenpolarization is reflected and the orthogonal polarization transmitted with near-unity efficiency and arbitrarily sharp frequency selectivity. When the incident light is circularly polarized, varying the eigenpolarization of the device tunes the amplitude and phase of reflected light of the same spin at will, opening totally new opportunities for Fano-based metasurfaces. By applying geometric phase concepts, we are able to realize ultrasharp resonant metasurfaces with arbitrary spatial phase profiles intrinsically encoded in an engineered dark mode with near-unity amplitude, ideal for highly spectrally and spin-selective wave front shaping. These results are deeply rooted in symmetries, implying that the concepts behind these generalized Fano resonances are not limited to flat optics applications but can be extended to a wide range of wave-based systems, from acoustics and radio frequencies to quantum photonics.

This work was supported by the DARPA SBIR program, Office of Naval Research, the National Science Foundation, the Simons Foundation and the Air Force Office of Scientific Research MURI program.

*Corresponding author.
aalu@gc.cuny.edu

†Corresponding author.
ny2214@columbia.edu

- [1] K. Koshelev, S. Lepeshov, M. Liue, A. Bogdanov, and Y. Kivshar, Asymmetric Metasurfaces with High-Q Resonances Governed by Bound States in the Continuum, *Phys. Rev. Lett.* **121**, 193903 (2018).
- [2] C. W. Hsu, B. Zhen, J. Lee, S.-L. Chua, S. G. Johnson, J. D. Joannopoulos, and M. Soljačić, Observation of trapped light within the radiation continuum, *Nature (London)* **499**, 188 (2013).
- [3] C. W. Hsu, B. Zhen, A. D. Stone, J. D. Joannopoulos, and M. Soljačić, Bound states in the continuum, *Nat. Rev. Mater.* **1**, 16048 (2016).
- [4] Z. Sadrieva, F. Frizyuk, M. Petrov, Y. Kivshar, and A. Bogdanov, Multipolar origin of bound states in the continuum, *Phys. Rev. B* **100**, 115303 (2019).
- [5] M. F. Limonov, M. V. Rybin, A. N. Poddubny, and Y. S. Kivshar, Fano resonances in photonics, *Nat. Photonics* **11**, 543 (2017).
- [6] C. J. Chang-Hasnain and W. Yang, High-contrast gratings for integrated optoelectronics, *Adv. Opt. Photonics* **4**, 379 (2012).
- [7] J. Jin, X. Yin, L. Ni, M. Soljačić, B. Zhen, and C. Peng, Topologically enabled ultrahigh-Q guided resonances robust to out-of-plane scattering, *Nature (London)* **574**, 501 (2019).
- [8] F. Lermarchand, A. Sentenac, E. Cambril, and H. Giovannini, Study of the resonant behavior of waveguide gratings: Increasing the angular tolerance of guided-mode filters, *J. Opt. Pure Appl. Opt.* **1**, 545 (1999).
- [9] Y. Wanf, J. Song, L. Dong, and M. Lu, Optical bound states in slotted high-contrast gratings, *J. Opt. Soc. Am. B* **33**, 2472 (2016).
- [10] H. S. Nguyen, F. Dubois, T. Deschamps, S. Cuffe, A. Pardon, J.-L. Leclercq, C. Seassal, X. Letartre, and P. Viktorovitch, Symmetry Breaking in Photonic Crystals: On-Demand Dispersion from Flatband to Dirac Cones, *Phys. Rev. Lett.* **120**, 066102 (2018).
- [11] A. C. Overvig, S. Shrestha, and N. Yu, Dimerized high contrast gratings, *Nanophotonics* **7**, 1157 (2018).
- [12] Y. Liang, W. Pend, R. Hu, and M. Lu, Symmetry-reduced double layer metallic grating structure for dual-wavelength spectral filtering, *Opt. Express* **22**, 11633 (2014).
- [13] A. C. Overvig, S. C. Malek, M. J. Carter, S. Shrestha, and N. Yu, Selection rules for quasibound states in the continuum, *Phys. Rev. B* **102**, 035434 (2020).
- [14] A. Tittl, A. Leitis, M. Liu, F. Yesilkoy, D.-Y. Choi, D. N. Neshev, Y. S. Kivshar, and H. Altug, Imaging-based molecular barcoding with pixelated dielectric metasurfaces, *Science* **360**, 1105 (2018).
- [15] C. Qui, J. Chen, Y. Xia, and Q. Xu, Active dielectric antenna on chip for spatial light modulation, *Sci. Rep.* **2**, 855 (2012).
- [16] S. Tibuleac and R. Magnusson, Reflection and transmission guided-mode resonance filters, *J. Opt. Soc. Am. A* **14**, 1617 (1997).
- [17] K. Koshelev, Y. Tang, K. Li, D.-Y. Choi, G. Li, and Y. Kivshar, Nonlinear metasurfaces governed by bound states in the continuum, *ACS Photonics* **6**, 1639 (2019).
- [18] A. Krasnok, M. Tymchenko, and A. Alù, Nonlinear metasurfaces: A paradigm shift in nonlinear optics, *Mater. Today* **21**, 8 (2018).
- [19] A. C. Overvig, S. C. Malek, and N. Yu, Multifunctional Nonlocal Metasurfaces, *Phys. Rev. Lett.* **125**, 017402 (2020).
- [20] C. Pfeiffer, C. Zhang, V. Ray, L. J. Guo, and A. Grbic, High Performance Bianisotropic Metasurfaces: Asymmetric Transmission of Light, *Phys. Rev. Lett.* **113**, 023902 (2014).
- [21] Y. Zhao, J. Shi, L. Sun, X. Li, and A. Alù, Alignment-free three-dimensional optical metamaterials, *Adv. Mater.* **26**, 1439 (2014).
- [22] A. N. Askarpour, Y. Zhao, and A. Alù, Wave propagation in twisted metamaterials, *Phys. Rev. B* **90**, 054305 (2014).

- [23] X. Piao, S. Yu, J. Hong, and N. Park, Spectral separation of optical spin based on antisymmetric Fano resonances, *Sci. Rep.* **5**, 16585 (2015).
- [24] A. V. Kondratov, M. V. Gorkunov, A. N. Darinskii, R. V. Gainutdinov, O. Y. Rogov, A. A. Ezhov, and V. V. Artemov, Extreme optical chirality of plasmonic nanohole arrays due to chiral Fano resonance, *Phys. Rev. B* **93**, 195418 (2016).
- [25] M. Moocarme, N. V. Proscia, and L. T. Vuong, Meta-optical chirality and emergent eigen-polarization modes via plasmon interactions, *Sci. Rep.* **7**, 40718 (2017).
- [26] J. Hu, X. Zhao, Y. Lin, A. Zhu, X. Zhu, P. Guo, B. Cao, and C. Wang, All-dielectric metasurface circular dichroism waveplate, *Sci. Rep.* **7**, 41893 (2017).
- [27] Y. Hwang, S. Lee, S. Kim, J. Lin, and X.-C. Yuan, Effects of Fano resonance on optical chirality of planar plasmonic nanodevices, *ACS Photonics* **5**, 4538 (2018).
- [28] F. Monticone, N. Mohammadi Estakhri, and A. Alù, Full Control of Nanoscale Optical Transmission with a Composite Metascreen, *Phys. Rev. Lett.* **110**, 203903 (2013).
- [29] C. Wu, N. Arju, G. Kelp, J. A. Fan, J. Dominguez, E. Gonzales, E. Tutuc, I. Brener, and G. Shvets, Spectrally selective chiral silicon metasurfaces based on infrared Fano resonances, *Nat. Commun.* **5**, 3892 (2014).
- [30] A. Zhu, W. T. Chen, A. Zaidi, Y.-W. Huang, M. Khorasaninejad, V. Sanjeev, C.-W. Qiu, and F. Capasso, Giant intrinsic chiro-optical activity in planar dielectric nanostructures, *Light* **7**, 17158 (2018).
- [31] Q. Yang, M. Liu, S. Kruk, Y. Xu, Y. K. Srivastava, R. Singh, J. Han, Y. Kivshar, and I. V. Shadrivov, Polarization-sensitive dielectric membrane metasurfaces, *Adv. Opt. Mater.* **8**, 2000555 (2020).
- [32] F. Zhang, M. Pu, X. Li, P. Gao, X. Ma, J. Luo, H. Yu, and X. Luo, All-dielectric metasurfaces for simultaneous giant circular asymmetric transmission and wavefront shaping based on asymmetric photonic spin-orbit interactions, *Adv. Funct. Mater.* **27**, 1704295 (2017).
- [33] K. Chen, G. Ding, G. Hu, Z. Jin, J. Zhao, Y. Feng, T. Jiang, A. Alù, and C. W. Qiu, Directional Janus metasurface, *Adv. Mater.* **32**, 1906352 (2020).
- [34] Z. Ma, Y. Li, Y. Li, Y. Gong, S. A. Maier, and M. Hong, All-dielectric planar chiral metasurface with gradient geometric phase, *Opt. Express* **26**, 6067 (2018).
- [35] S. Carr, D. Massat, S. Fang, P. Cazeaux, M. Luskun, and E. Kaxiras, Twistronics: Manipulating the electronic properties of two-dimensional layered structures through their twist angle, *Phys. Rev. B* **95**, 075420 (2017).
- [36] G. Hu, A. Krasnok, Y. Mazar, C.-W. Qiu, and A. Alù, Moire hyperbolic metasurfaces, *Nano Lett.* **20**, 3217 (2020).
- [37] G. Hu, Q. Ou, G. Si, Y. Wu, J. Wu, Z. Dai, A. Krasnok, Y. Mazar, Q. Zhang, Q. Bao, C.-W. Qiu, and A. Alù, Observation of topological polaritons and photonic magic angles in twisted van der Waals bi-layers, *Nature (London)* **582**, 209 (2020).
- [38] See Supplemental Material at <http://link.aps.org/supplemental/10.1103/PhysRevLett.126.073001> for more discussion on the properties of QBICs, a detailed derivation of coupled mode theory for this system, a derivation of Eq. (2), and construction of the look-up table for the metasurface library.
- [39] S. Fan, W. Suh, and J. D. Joannopoulos, Temporal coupled-mode theory for the Fano resonance in optical resonators, *J. Opt. Soc. Am. A* **20**, 569 (2003).
- [40] Y. Zhao, M. A. Belkin, and A. Alù, Twisted optical metamaterials for planarized ultrathin broadband circular polarizers, *Nat. Commun.* **3**, 870 (2012).
- [41] Y. Zhou, I. I. Kravchenko, H. Wang, H. Zheng, G. Gu, and J. Valentine, Multifunctional metaoptics based on bilayer metasurfaces, *Light* **8**, 80 (2019).
- [42] A. C. Overvig, S. Shrestha, S. C. Malek, M. Lu, A. Stein, C. Zheng, and N. Yu, Dielectric metasurfaces for complete and independent control of the optical amplitude and phase, *Light* **8**, 92 (2019).
- [43] W. Liu, B. Wang, Y. Zhang, J. Wang, M. Zhao, F. Guan, X. Liu, L. Shi, and J. Zi, Circularly Polarized States Spawning from Bound States in the Continuum, *Phys. Rev. Lett.* **123**, 116104 (2019).
- [44] H. M. Doeleman, F. Monticone, W. den Hollander, A. Alù, and A. F. Koenderink, Experimental observation of a polarization vortex at an optical bound state in the continuum, *Nat. Photonics* **12**, 397 (2018).